ELSEVIER

Chemical Engineering Science 61 (2006) 676–687

Chemical Engineering Science

www.elsevier.com/locate/ces

CFD modelling of slug flow in vertical tubes

Taha Taha, Z.F. Cui*

Department of Engineering Science, Oxford University, Parks Road, Oxford OX1 3PJ, UK

Received 15 June 2004; received in revised form 4 July 2005; accepted 6 July 2005
Available online 12 September 2005

Abstract

In this work we present a numerical study to investigate the motion of single Taylor bubbles in vertical tubes. A complete description of the bubble propagation in both stagnant and flowing liquids was obtained. The shape and velocity of the slug, the velocity distribution and the distribution of local wall shear stress were computed and compared favourably with the published experimental findings. The volume of fluid (VOF) method implemented in the commercial CFD package, Fluent is used for this numerical study.

Keywords: Multiphase flow; Vertical slug flow; Numerical simulation; VOF

1. Introduction

When gas and liquid flow in a pipe they tend to distribute themselves in a variety of configurations. These characteristic distributions of the fluid–fluid interface are called flow patterns or flow regimes. Much time and effort has been expended in determining these regimes for various pairs of fluids, channel geometries, and inclinations (Mandhane et al., 1974; Taitel and Duckler, 1976; Taitel, 1986; Barnea, 1987). For vertical co-current flow and at low gas flow rates, the flow pattern observed is bubbly. Here, the gas phase is distributed as discrete bubbles within the liquid continuum. At higher gas flow rates, some of the bubbles have nearly the same cross-sectional area as that of the channel. These bullet-shaped bubbles—sometimes referred to as 'Taylor bubbles' or 'slugs'—move along and are separated by liquid plugs that may or may not contain a dispersion of smaller gas bubbles. An increase in the gas flow rate in a two-phase mixture flowing in slug flow will eventually result in a complete destruction of slug flow integrity with consequential churning or oscillatory action. At very high gas flow rates, the flow becomes annular, in which, adjacent to the channel wall. There is a liquid continuum and the core of the channel is a gas continuum (Hewitt and Hall-Taylor, 1970).

Slug flow is the most important of the two-phase flow regimes primarily because of the numerous industrial and practical applications. Some of these include buoyancy-driven fermenters, production and transportation of hydrocarbons, boiling and condensation processes in thermal power plants, and emergency cooling of nuclear reactors. Slug flow is characterised by its random intermittence and inherent unsteadiness. A fixed observer would see a quasi-periodic occurrence of long, bullet-shaped Taylor bubbles followed by liquid plugs sometimes carrying dispersed bubbles and taking on the appearance of bubbly flow in a pipe. The bubble region may take on stratified or annular configurations depending upon the tube inclination and flow conditions. In order to understand the complex features of intermittent slug flow, mainly experimental research has been conducted to study the motion of isolated Taylor bubbles in motionless and flowing liquids for various inclination angles. Here, vertical slug flow will be emphasised.

The shape and the velocity with which a single Taylor bubble ascending through a denser stagnant liquid is influenced by the forces acting on it, namely the viscous, inertial and interfacial forces. Dimensionless analysis based on Pi-theorem leads to the following dimensionless

* Corresponding author. Tel.: +44 1865 273118; fax: +44 1865 283273.
E-mail address: zhanfeng.cui@eng.ox.ac.uk (Z.F. Cui).

0009-2509/$ - see front matter © 2005 Elsevier Ltd. All rights reserved.
doi:10.1016/j.ces.2005.07.022

groups:

$$\frac{U_{TB}^2\rho_L}{gD_t(\rho_L-\rho_G)}\frac{g(\rho_L-\rho_G)D_t^2}{\sigma},$$
$$\frac{g\mu_L^4(\rho_L-\rho_G)}{\rho_L^2\sigma^3},\frac{\rho_L}{\rho_G},\frac{\mu_L}{\mu_G},\frac{L_{TB}}{D_t},$$

where D_t is the diameter of the tube, U_{TB} is Taylor bubble velocity, ρ_L and ρ_G are the density of the liquid and gas, respectively, μ_L and μ_G are the viscosity of the liquid and gas respectively, σ is the surface tension and L_{TB} is the length of Taylor bubble. For cylindrical bubbles, the film thickness and the bubble rise velocity are independent of the bubble length (Griffith and Wallis, 1961; Nicklin et al., 1962; Mao and Duckler, 1989; Polonsky et al., 1999). Under the assumption that inertial forces in the gas are far smaller than the inertial forces in the liquid ($\rho_L/\rho_G \gg 1$), ρ_L/ρ_G can be eliminated. And if the viscosity of the gas in the bubble is neglected the following set of three dimensionless groups is sufficient to characterise the motion of a single bubble rising through a motionless liquid. These are the Eötvös number $Eo = g(\rho_L - \rho_G)D_t^2/\sigma$, the Morton number defined as $M = g\mu_L^4(\rho_L-\rho_G)/\rho_L^2\sigma^3$ and the Froude number defined as $Fr = U_{TB}/\sqrt{gD_t(\rho_L-\rho_G)/\rho_L}$. The Eötvös number represents the relative significance of surface tension and buoyancy. The Morton number is sometimes referred to as the property group. The Froude number represents the ratio of inertial to gravitational forces. Other dimensionless groups could be used, e.g., Fabre and Line (1992) in their review paper on the motion of Taylor bubbles used Froude number as a unique function of Eötvös number and a dimensionless inverse viscosity number, N_f, given by $N_f = (gD_t^3)^{1/2}/v$. Wallis (1969) used a set of Fr, N_f and Archimedes number Ar ($Ar = \sigma^{3/2}\rho_L/\mu_L^2 g^{1/2}(\rho_L - \rho_G)^{1/2}$). Other and these widely used dimensionless groups can all be derived by manipulating and/or combining two or more of groups adopted in this work, e.g., $N_f = (E_o^3/M)^{1/4}$, $Ar = (1/M)^{1/2}$ and the capillary number, $Ca = Fr(M\,Eo)^{1/4}$ which is the ratio of viscous to surface tension forces. White and Beardmore (1962) described a wide spectrum of experimental results on Taylor bubbles drifting through motionless liquids in vertical tubes. The authors presented a cross plot (Fig. 6 in their paper) showing the regions in which various retarding forces may be neglected. The density of air was neglected and instead of Fr, $\sqrt{Fr}$ is plotted to have a reasonable spread of data (White and Beardmore, 1962). In the region where surface tension dominates the bubble does not move at all where the hydrostatic forces are completely balanced by surface tension forces. This occurs at $Eo < 3.37$ (Hattori, 1935; Bretherton, 1961). For inertia-controlled region when viscosity and surface tension can be neglected ($Eo > 100$, $N_f > 300$, $\rho_L^2 g D_t/\mu_L^2 > 3 \times 10^5$), the bubble rise velocity is given solely in terms of Fr (Nicklin et al., 1962; White and Beardmore, 1962; Zukoski, 1966; Mao and Duckler, 1990). In the centre of the graph, the relative magnitude of all retarding forces, namely the viscous, inertial, and interfacial forces are significant. In this region the relationship between Fr, Eo, and M for vertical tubes has been presented by White and Beardmore (1962) as a graphical map which plots lines of constant M on Fr–Eo axis. Similar maps have been produced for non-vertical tubes by Wallis (1969) and Weber et al. (1986).

The description of the motion of single Taylor bubbles in flowing liquids dates back to the pioneering work of Nicklin's et al. (1962) who placed the corner stone of slug flow modelling by recognising the fact that the bubble velocity is a superimposition of two components:

$$U_{TB} = C_1 U_m + U_0. \quad (1)$$

The second term represents the drift due to buoyancy (the bubble velocity in a stagnant liquid) and the first term refers to the transport by the mean flow, U_m ($U_m = U_{SL} + U_{SG}$). C_1 is a dimensionless coefficient that depends on the velocity profile ahead of the bubble, and can be seen as the ratio of the maximum to the mean velocity in the profile. Hence for turbulent flows, $C_1 \cong 1.2$ while for laminar pipe flow, $C_1 \cong 2$ (Nicklin et al., 1962; Collins et al., 1978; Grace and Clift, 1979; Bendiksen, 1985; Polonsky et al., 1999). The velocity field around the bubble has been measured by many researchers primarily because of its importance regarding the interaction between two Taylor bubbles. Several techniques have been adopted, e.g.: the photochromic dye activation (PDA) method (DeJesus et al., 1995; Kawaji et al., 1997; Ahmad et al., 1998), the particle image velocimetry (PIV) technique (Polonsky et al., 1999; Nogueria et al., 2000) and the laser doppler velocimetry (LDV) technique (Kvernvold et al., 1984). Measurement of wall shear stress in stagnant (Mao and Duckler, 1989) and flowing (Nakoryakov et al., 1989) water showed clearly the reversal of the flow in the liquid film. Experimental work on the propagation of Taylor bubbles in downward flow has been limited to a few studies on ascending bubbles in vertically downward flow (Martin, 1976; Polonsky et al., 1999) and one single study (to our knowledge) on inclined downward flow by Bendiksen (1984). Theoretical treatments of the problem for predicting the rise bubble velocity have been successful for the special case of vertical tubes. This is, however, restricted to the case where both viscous and surface tension effects are negligible (Dumitrescu, 1943; Davies and Taylor, 1950), or the case where viscous effects dominate (Goldsmith and Mason, 1962). Later, Bendiksen (1985) extended the theoretical approach of Dumitrescu (1943) and Davies and Taylor (1950) to account for the surface tension. Mao and Duckler (1990, 1991) and Clarke and Issa (1997) performed numerical simulations in order to calculate the velocity of the bubble and the velocity field in the liquid film. Propagation of Taylor bubbles in non-vertical tubes has been less well studied experimentally, and even less well theoretically, for the obvious reason of asymmetry.

Thus, studying the motion of a single Taylor bubble in stagnant and in moving liquid is essential in order to understand the intrinsically complicated nature of slug flow.

The rise of a single bubble in both stagnant and flowing liquid inside vertical tubes has been extensively studied by numerous researchers, both experimentally and theoretically. All the published numerical methods to model slug flow are restricted only to vertical tubes and they assume either the shape of the bubble or a functional form for the shape (Dumitrescu, 1943; Davies and Taylor, 1950). These assumptions constrain the nature of the solution, while the approach adopted here (the volume of fluid method, VOF) lays no such a priori foundations. The solution domain in the present model not only includes the field around the bubble, as in the study of Mao and Duckler (1990), but also extends behind the bubble, allowing field information to be obtained in the wake region. The difficulty of obtaining local data is even more complicated in horizontal and inclined slug flow by the fact that the flow is asymmetric, and consequently, very few detailed data have been published in the open literature. Previous models available in literature also fail to provide a fully satisfactory mechanistic model of slug flow in horizontal configuration (Duckler and Hubbard, 1975; Taitel and Barnea, 1990). Thus, it is evident that more insight into slug flow is needed to attain a thorough understanding of the internal structure of the slug flow pattern. In this work, an attempt is made to calculate the shape and rising velocity of a single Taylor bubble in stagnant and in moving liquid in vertical tubes. The velocity field in a slug unit (Taylor bubble + liquid plug) and wall shear stress are also calculated. The intention of future work is to characterise the hydrodynamics of slug flow when the tube is tilted away from the vertical and also to investigate the effect of the leading bubble on the shape and velocity of the trailing one.

2. CFD model development

The CFD software FLUENT (Release 5.4.8, 1998) is used to simulate the motion of a single Taylor bubble rising in a motionless or flowing liquid through a vertical tube. In FLUENT, the control volume method—sometimes referred to as the finite volume method—is used to discretise the transport equations. The movement of the gas–liquid interface is tracked based on the distribution of α_G, the volume fraction of gas in a computational cell, where $\alpha_G = 0$ in the liquid phase and $\alpha_G = 1$ in the gas phase (Hirt and Nichols, 1981). Therefore, the gas–liquid interface exists in the cell where α_G lies between 0 and 1.

2.1. Model geometry

For axisymmetric simulations, a 2D coordinate system assuming axial symmetry about the centreline of the pipe is used. The length of the domain is $11D_t$, where D_t is the tube diameter. The grids used to generate the numerical results throughout this work are either uniform grids containing quadrilateral control elements/volumes or uniform grids with extra refinement near the walls. Confidence of grid independence results is gained by selecting simulations that were run with the grid cells number doubled (i.e., choosing results from a 52×560 grid rather than a 26×280). Prior to simulations simple mass balance was performed to test whether the film is turbulent. This is discussed below. For axisymmetric simulations, the grid was uniform containing 52×560 *elements* when the liquid film is laminar. If the liquid film is turbulent, the last row of cells near the walls is sub-divided three times. The result is a 59×560 *elements* in the domain. This refinement method, ensuring film region grid independence, does, however, not always guarantee full grid independence in regions where the air–liquid interface is highly curved.

In Fig. 1 the boundary conditions and the initial bubble shape used in the simulation are displayed. The initial bubble shape consists of one hemisphere connected to a cylinder of the same radius. If other shapes were used (e.g. only a cylinder), the final shape of the bubble is found to be similar except the convergence is slower in the latter case. Thus, for the simulations the former initial shape is adopted. The initial guess for the film thickness and the bubble rise velocity are calculated using simple mass balance and Eq. (1), respectively. The no-slip wall condition is applied to the walls. The fluid mass flux at the inlet is specified using a profile for a fully developed flow through a pipe. The governing equations are solved for a domain surrounding a Taylor bubble in a frame of reference attached to the rising Taylor bubble. With these coordinates, the bubble becomes stationary and the pipe wall moves with a velocity U_{wall}, equal to that of the Taylor bubble rise velocity, U_{TB}. The liquid is fed at the inlet with an average velocity U_{inlet}, which is equal to $U_{TB} - U_{SL}$. A fully developed velocity profile is imposed at the inlet and the relative movement between the liquid and the wall generates a velocity profile shown in Fig. 1. The value of U_{TB} is adjusted after the initial guess until the nose of the bubble ceased to move in the axial direction. Trial simulations were conducted to examine the effect of using a fixed frame of reference; they run longer with the same final result as with that of a moving frame of reference. Throughout this work moving wall simulations are presented. The frame of reference, initial and the boundary conditions for 3D simulations are similar to those adopted in axisymmetric simulations. The geometric reconstruction scheme that is based on the piece linear interface calculation (PLIC) method of Youngs (1982) is applied to reconstruct the bubble free surface. The surface tension is approximated by the continuum surface force model of Brackbill et al. (1992). In all calculations, Courant number was set to a value of 0.25 and time step was set to 10^{-3} s.

2.2. Turbulence model and grid refinement

Prior to simulations a simple momentum and mass balance (Taitel and Barnea, 1990) was conducted to test whether the liquid film is turbulent. The RNG k-epsilon model was the

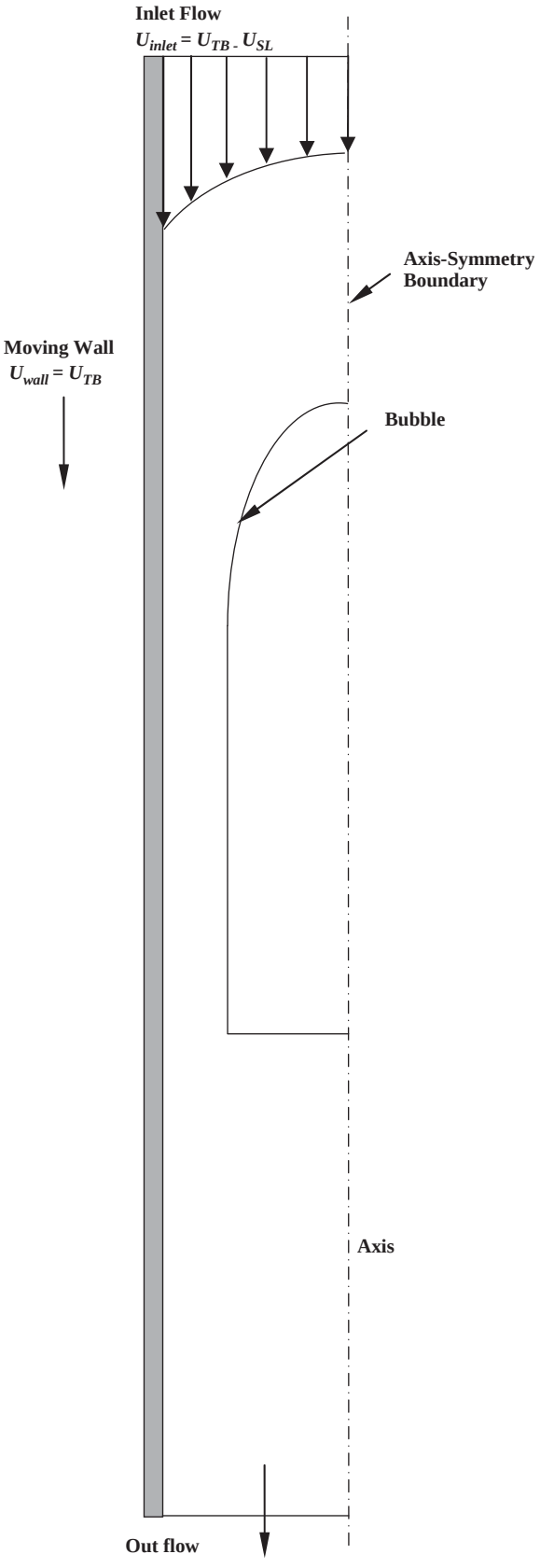

Fig. 1. Initial and boundary conditions for a Taylor bubble rising in a vertical pipe in a moving coordinate moving with the bubble.

turbulence model used throughout this work. A mass balance on the liquid film, relative to a coordinate system moving with the bubble, yields the following differential equation:

$$\frac{dU_f}{dx} = -\left\{\left[\frac{g(1-\rho_L/\rho_G)}{(U_{TB}-U_f)} + \frac{(2/D_t)f_w}{(U_{TB}-U_{SL})}\right] \times U_f|U_f|\right\}, \quad (2)$$

where $f_w = C_f(D_t F_f U_f \rho_L/\mu_L)^m$, F_f being the liquid holdup in film which can be written as a function of liquid film thickness, $F_f = 2h/R - h^2/R^2$ where h is the liquid film thickness and R is the tube radius. For laminar flow $C_f = 16$ and $m = -1$, while for turbulent flow $C_f = 0.046$ and $m = -0.2$. The above differential equation was solved using a 4th Runge–Kutta with initial condition: $U_f = U_{SL}$ at $x = 0$ where x is axial distance from the bubble nose. This will give us the local liquid film thickness, $h(x)$ and the local film velocity, $U_f(x)$. When the flow is turbulent in the film ($Re_f > 2000$), a turbulence model is introduced (Taitel and Barnea, 1990).

3. Results and discussion

3.1. Drift of Taylor bubbles in stagnant liquids

Consider a single Taylor bubble rising in stagnant liquid inside a vertical tube with velocity U_{TB}. The bubble may be made stationary by superimposing a downward velocity U_{TB} to the liquid and to the tube walls. The bubble has a round nose and fills almost the cross sectional area of the tube (Fig. 2). The liquid ahead of the bubble moves around the bubble as a thin liquid film moving downwards in the annular space between the tube wall and the bubble surface. Alongside the bubble, the liquid film accelerates until it reaches its terminal velocity under the condition of a long enough bubble. At the rear of that bubble, the liquid film plunges into the liquid plug behind the bubble as a circular wall jet and produces a highly agitated mixing zone in the bubble wake. As shown clearly in Fig. 2, this recirculation zone sometimes contains small bubbles shed from the bubble tail due to the turbulent jet of the liquid film.

Experimental data obtained by extensively varying the fluid properties and pipe diameter, indicated that the terminal rising velocity and shape are significantly affected by viscosity, surface tension, buoyancy and inertia. By taking into account these effects, White and Beardmore (1962) conducted a dimensional analysis using a large matrix of experimental data. They also proposed a graphical correlation of the terminal rise velocity of Taylor bubble inside vertical tubes. The three dimensionless numbers, *Eo*, *M* and *Fr*, are the Eötvös, Morton and Froude numbers, respectively, defined above. Fig. 3 presents the computed results for water where the Froude number is plotted as a function of Eötvös and $M < 10^{-8}$. It can be seen that the results agree well

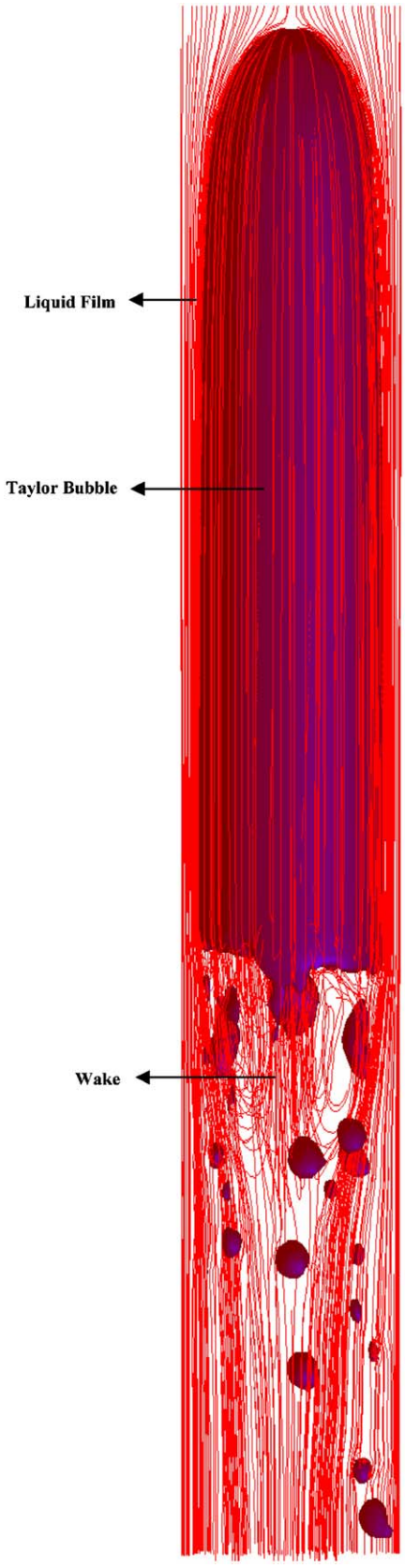

Fig. 2. Numerical simulation of a Taylor bubble rising through glycerine in a vertical tube.

with a wide range of experimental results and correlations reported in literature. For low viscous liquids, all the data points reported follow the same course where there is a critical *Eo* value ($Eo < 3.37$) below which the bubble ceased to move. Increasing *Eo* would increase the bubble velocity as Eötvös number represents the relative significance of surface tension and buoyancy. For more viscous liquids, the calculated terminal rise velocity of a Taylor bubble in several liquids covering a wide range of Eötvös and Morton numbers is presented in Fig. 4, where the results compared favourably with experimental data reported by White and Beardmore (1962). In Fig. 4 the separation of the curves can be attributed to the increasing importance of viscous forces on the terminal rise velocity.

Goldsmith and Mason (1962) observed in their experiments that in the case of high viscosity both ends of the bubble rising in stagnant liquid are spheroids; the top end is prolate and the bottom is oblate. They also indicated that the degree of prolateness of the nose and oblateness of the tail increase with surface tension. In addition, they reported that a wave disturbance would appear at the tail of the bubble when the viscosity is high. Also, the film thickness decreases as the surface tension increases. Fig. 5 shows the results from the VOF method of the effects of *Eo* and *M* on the bubble shape. With decreasing Morton number under a constant Eötvös number, the bluntness of the nose of the bubble increases and the bubble tail is flattening, which results in an increment of the liquid film thickness around the bubble. The bluntness of the nose increases with increasing *Eo*. The wavelet disturbance shown in Fig. 5 appears when *Eo* is low. In the above calculations, it is found that the film thickness and the bubble rise velocity are independent of the bubble length, which is consistent with experiments by other researchers (Griffith and Wallis, 1961; Nicklin et al., 1962).

The understanding of the hydrodynamic characteristic of wake behind the bubble is of great importance to the task of modelling transient slug flow (Moissis and Griffith, 1962; Duckler et al., 1985; Fabre and Line, 1992). The wake region is believed to play a pivotal role in explaining the interaction and coalescence between two successive Taylor bubbles (Moissis and Griffith , 1962; Shemer and Barnea , 1987; Taitel and Barnea, 1990; Pinto and Campos, 1996; Talvy et al., 2000). For situations where heat and mass transfer is augmented by introducing air slugs this understanding can be critical.

Inspired by the work of Maxworthy (1967), Campos and Guedes de Carvalho (1988) conducted a photographic study of the wake behind Taylor bubble. The liquids used were water, glycerol, and mixture of the two in different proportions, covering a wide range of viscosities. The authors adopted *Fr*, N_f and *Eo* as the set of dimensionless group to characterise the wake pattern behind the bubbles. In their experiments the surface tension may be neglected ($Eo > 680$) and for $N_f > 250$ the Froude number, $Fr = 0.351$. Thus the wake nature depends solely on the dimensionless number, N_f (Campos and Guedes de Carvalho,

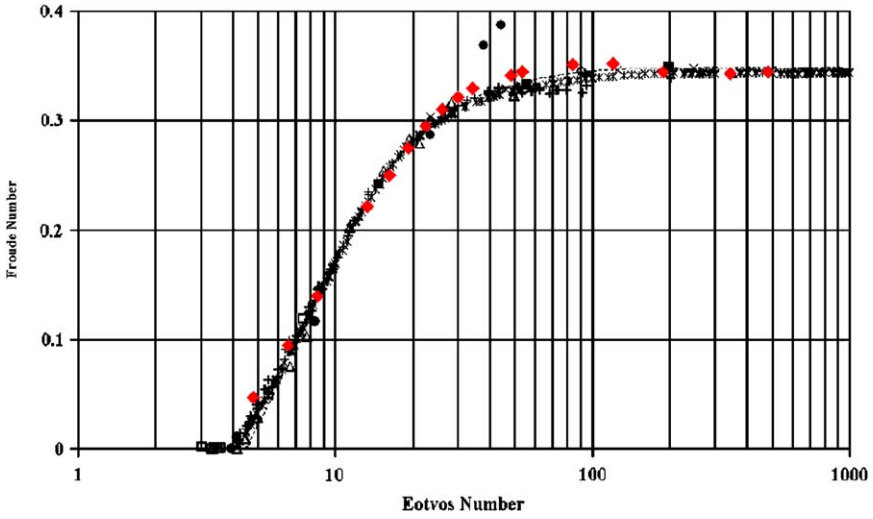

Fig. 3. Taylor bubble rise velocity in stagnant water and dilute aqueous solutions contained in vertical tubes: (■) Dumitrescu (1943); (▲) Laird and Chisholm (1956); (●) Gibson (1913); (□) Barr (1926); (△) Hattori (1935); (○) Nicklin et al. (1962); (×) Griffith and Wallis (1961); (+) White and Beardmore (1962); (✱) White Correlation (1962); (.....) Harmathy Correlation (Harmathy, 1960); (◇) Polonsky et al. (1999); (⧫) CFD-This work.

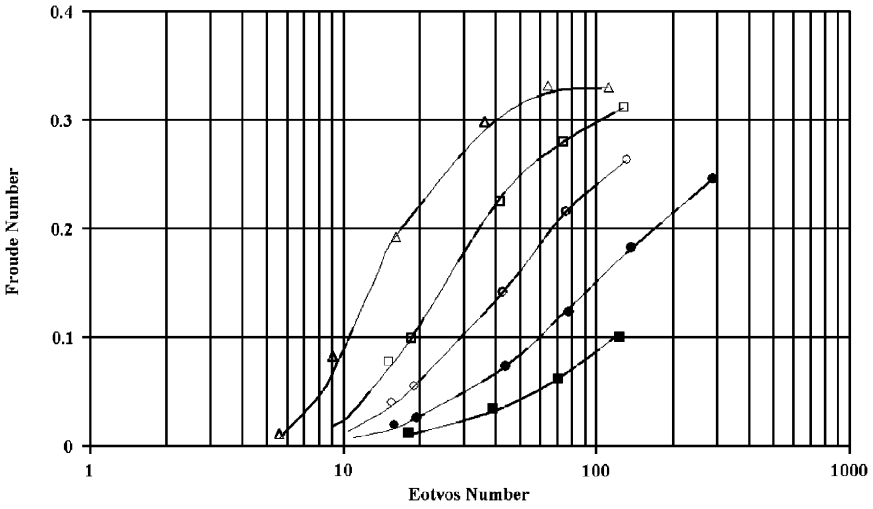

Fig. 4. Taylor bubble rise velocity in stagnant viscous liquids contained in vertical tubes, experiment, White and Beardmore (1962): (△) $M = 4.7 \times 10^{-5}$; (□) $M = 1.6 \times 10^{-2}$; (○) $M = 0.33$; (●) $M = 8.0$; (■) $M100$; (—) CFD-This work.

1988). They identified three different patterns in the wake depending on N_f. The authors observed a closed axisymmetric wake for $N_f < 500$, closed unaxisymmetric wake for $500 < N_f < 1500$ and opened wake with recirculatory flow for $N_f > 1500$. Their experimental results are simulated here. The wake patterns for five different N_f values are presented in Fig. 6. For lowest value of N_f, the annular film conforms to the body of the tail of the bubble. With increasing N_f, the liquid jet starts to separate from the body of the bubble with the free streamlines rejoining together at some point downstream forming a closed region, i.e., the wake, containing closed vortices travelling steadily at the same velocity of the bubble. The wake here is enclosed into the oblate tail of the bubble and is axisymmetric with respect of the tube axis. No bubble shedding is observed. Campos and Guedes de Carvalho (1988) observed the same type of pattern and they referred to them as laminar wakes. Increasing N_f further causes the wake to stretch downstream. At high N_f, the free streamlines may not rejoin downstream resulting in an open wake thereby allowing for vortex shedding. Here, 3D simulation of the bubble is conducted to capture the 3D nature of the flow. The unstable and transient nature of the flow surrounding the bubble from laminar to turbulent produces significant modification to the bubble profile and stability. As one can see from Fig. 6 the bubble tail oscillates and small bubbles can be seen shed at the bubble rear. Fig. 7 depicts a sequence of pictures of a 3D shape of the bubble and the velocity field around it obtained with a

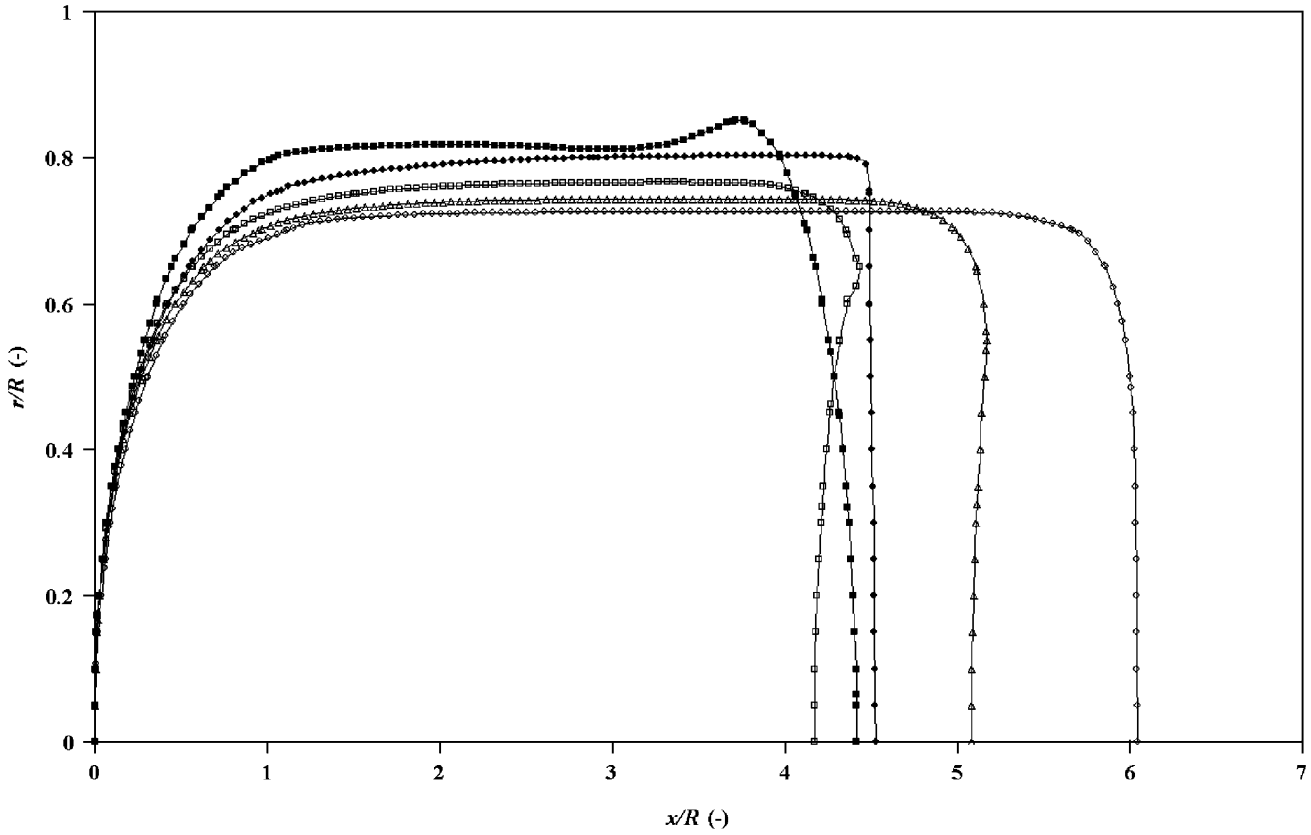

Fig. 5. Bubble shape profile: (■)Eo=477, $M=4.7\times10^{-5}$; (●) Eo=120, $M=4.7\times10^{-5}$; (□) Eo=1986, $M=1.6\times10^{-2}$; (△) Eo 1142, $M=1.6\times10^{-2}$; (○) Eo = 642, M 1.6×10^{-2}; bubble volume = 1.03 ml; x—axial distance from bubble nose.

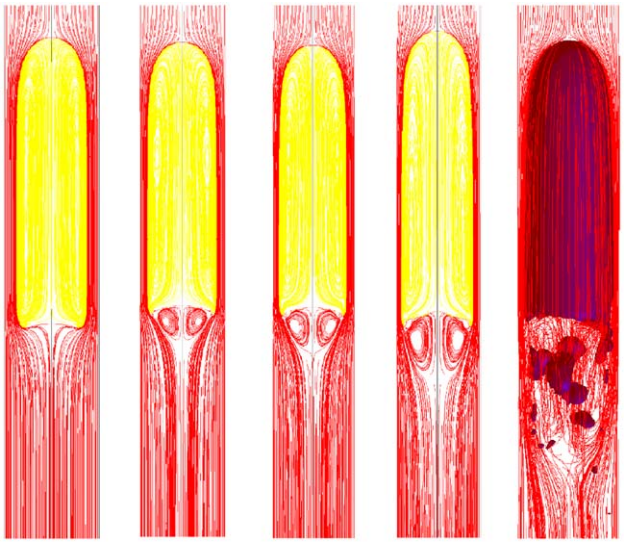

Fig. 6. Wake flow pattern at different values of N_f for bubbles rising through stagnant glycerol solutions inside a 19 mm vertical tube; the frame of reference is moving with the bubble: (a) $\rho=1223\,kg/m^3$; $v=9.7\times10^{-5}\,m^2/s$; Eo=0.066; Fr=0.30; N_f=84, (b) $\rho=1206\,kg/m^3$; $v=4.67\times10^{-5}\,m^2/s$; Eo = 0.064; Fr = 0.341; N_f = 176, (c) $\rho=1202\,kg/m^3$; $v=4.0\times10^{-5}\,m^2/s$; Eo=0.064; Fr=0.351; N_f=205, (d) $\rho=1190\,kg/m^3$; $v=2.5\times10^{-5}\,m^2/s$; Eo=0.063; Fr=0.351; N_f=325, (e) $\rho=1129\,kg/m^3$; $v=547\times10^{-6}\,m^2/s$; Eo=0.064; Fr=0.341; N_f=1528.

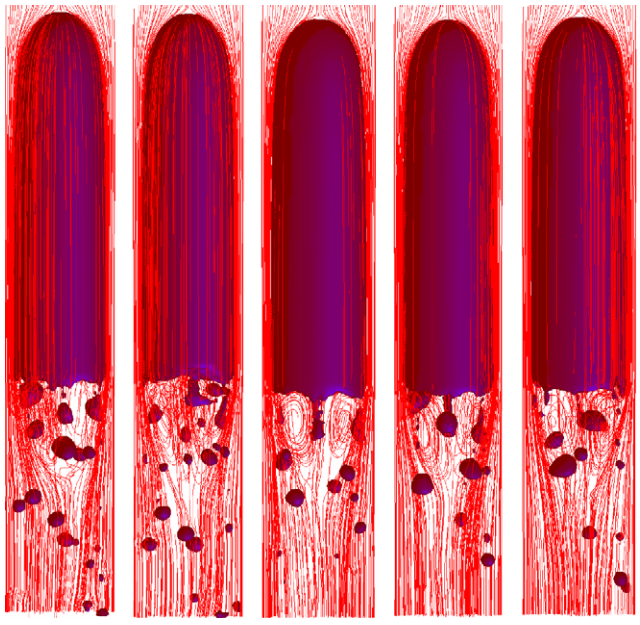

Fig. 7. Progression of wake flow pattern behind a Taylor bubble rising through a stagnant glycerol solution inside a 19 mm vertical tube: $\rho=1181\,kg/m^3$; $v=1.9\times10^{-5}\,m^2/s$; Eo=0.062; Fr=0.351; N_f=437; Δt = 0.01 s; the frame of reference is moving with the bubble.

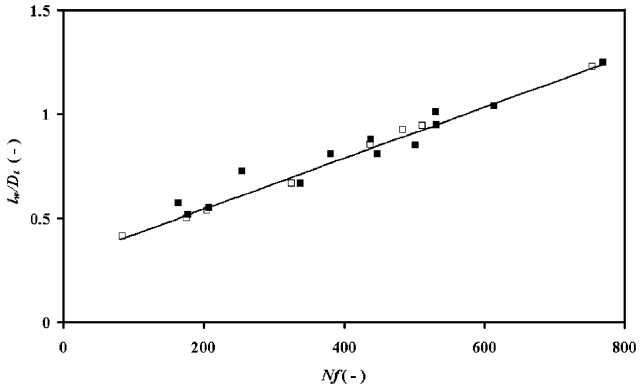

Fig. 8. Dependence of length of bubble wake on N_f: (□) numerical results; the liquids used are stagnant glycerol solutions similar to those presented in Fig. 5, $D_t = 19$ mm; (■) experiment, Campos and Duedes de Carvalho (1988); (—) correlation, Campos and Duedes de Carvalho (1988).

time interval of 0.01 s between the consecutive images at moderate N_f. It can be seen that the bubble nose propagates smoothly, while the tail is characterised by vigorous oscillations accompanied by small bubbles being shed at the bubble trailing end. This was observed experimentally by Polonsky et al. (1999). The wake of the bubble is closed but lacks symmetry and it tends to oscillate and was referred to as transitional wake by Campos and Guedes de Carvalho (1988). Fig. 7 also shows that a streaming tail can be seen trailing the travelling transitional wake in accordance with the experimental findings by Lighthill (1968). The dependence of wake length on N_f for low and intermediate N_f is depicted in Fig. 8. The length of the wake is defined as the distance between the bottom of the bubble at the central plane of the tube and the stagnation area behind the bubble (Nogueria et al., 2000). The linear relationship between the wake length and N_f suggested by the Campos and Guedes de Carvalho (1988) is plotted together with their experimental results and compared favourably with the theoretical values.

Fig. 9 illustrates the calculated wall shear stress around a slug unit (Taylor bubble + liquid plug) for a bubble rising into stagnant glycerol solutions inside a 19 mm diameter tube at different values of N_f. The frame of reference is as seen by a fixed observer and not moving with the bubble. The shear stress is plotted against a dimensionless distance from the bubble nose. The character of the wall shear stress distribution is similar for all cases. The wall shear stress rapidly increases attaining its maximum positive value, indicating downflow in the film, near the bubble tail and then starts to decrease to zero at the end of the bubble wake. The positive value of the shear stress just ahead of the bubble indicates the existence of upward flow upstream of the bubble nose. This bubble expansion-induced velocity is confined to approximately $0.5D_t$ ahead of the bubble in agreement with Polonsky et al. (1999) and van Hout et al. (2002). The falling liquid film is accelerated under gravity along the Taylor bubble while the film thickness is continually narrowed (Fig. 10) until it is stabilised under the action of the friction force at the wall provided that the bubble is long enough. In this case the film attains its terminal film thickness and the corresponding terminal velocity. Figs. 9 and 10 suggest that the distance from the bubble nose where the liquid film reaches its terminal thickness and velocity increases with increasing N_f. Increasing N_f also results in an increase in the wall shear stress and a reduction in the liquid film thickness.

3.2. Rise of Taylor bubbles in flowing liquids

For a Taylor bubble rising in a moving liquid it is generally agreed that the translational bubble velocity, U_{TB}, can be expressed as the superimposition of two components: the

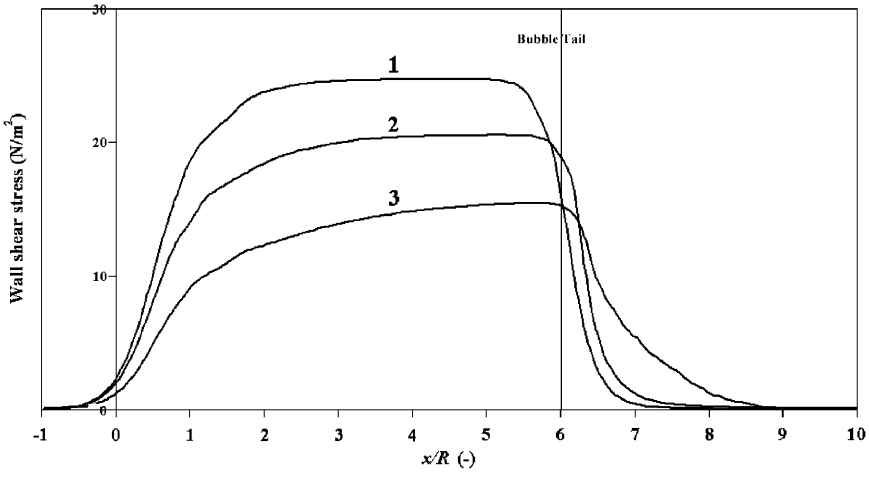

Fig. 9. Wall shear stress distribution in a slug unit at different values of N_f : $D_t = 19$ mm; liquids used are stagnant glycerol solutions; 1- $N_f = 84$, $Eo = 0.066$; 2-$N_f = 176$, $Eo = 0.065$; 3- $N_f = 437$, $Eo = 0.062$; bubble length $= 3D_t$; x—axial distance from bubble nose; the frame of reference is as seen by a fixed observer.

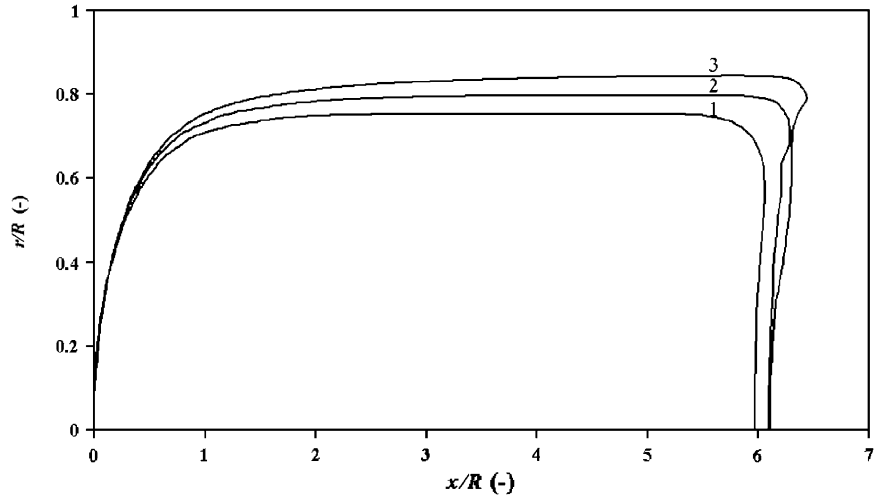

Fig. 10. Bubble shape profile at different values of N_f : $D_t = 19$ mm; liquids used are stagnant glycerol solutions; 1- $N_f = 84$, $Eo = 0.066$; 2- $N_f = 176$, $Eo = 0.065$; 3- $N_f = 437$, $Eo = 0.062$; x—axial distance from bubble nose.

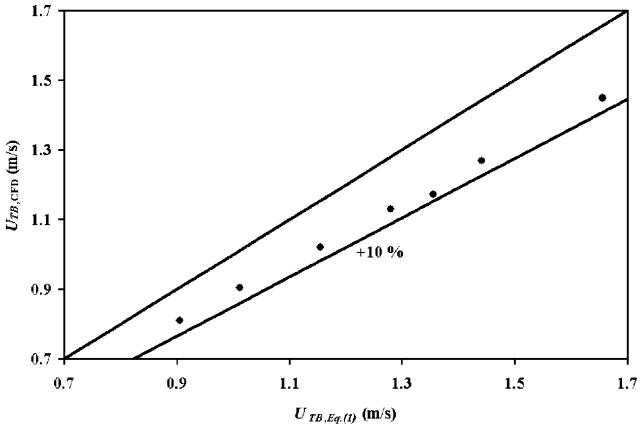

Fig. 11. Parity plot of Taylor bubble velocity: $D_t = 20$ mm; air–water system.

drift due to buoyancy (the bubble velocity in a stagnant liquid) and the velocity due to the transport by the mean flow (Eq. (1)). It is generally assumed that the value of $C_1 U_m$ is equal to the maximum local superficial liquid velocity (Nicklin et al., 1962; Collins et al., 1978). Thus, for turbulent pipe flow, $C_1 \approx 1.2$, while for a fully developed laminar flow in a pipe the value of C_1 approaches 2. The bubble propagation velocity inside a 20 mm diameter tube was calculated and found to be $U_0 = 0.155$ m/s, corresponding to $0.351\sqrt{g D_t}$, which is in agreement with Dumitrescu (1943) and Nicklin et al. (1962). Fig. 11 shows a parity plot of the translational bubble velocity predicted by Eq. (1) and the calculated values with reasonable agreement.

Fig. 12 illustrates the calculated wall shear stress around a slug unit for various superficial liquid velocities for a Taylor

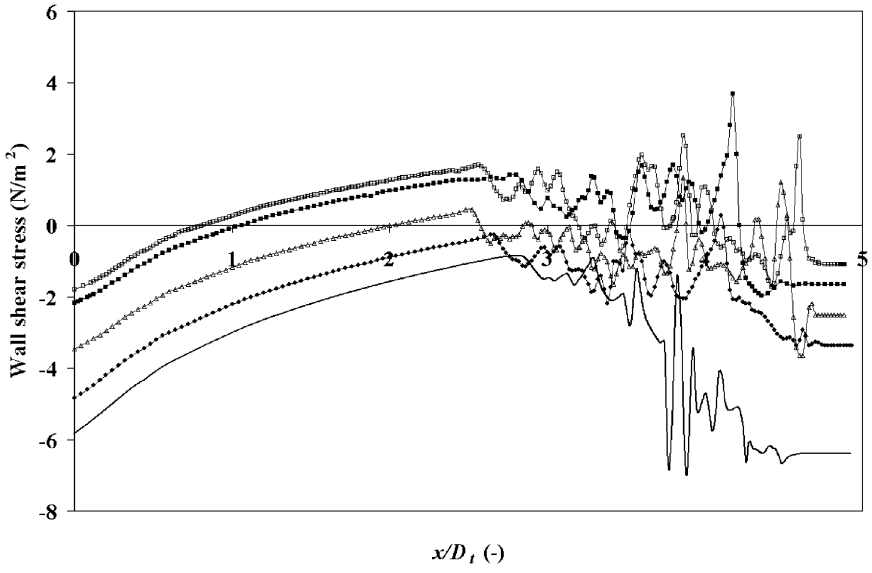

Fig. 12. Wall shear stress distribution in a slug unit: $D_t = 20$ mm; air–water system; (□) $U_{SL} = 0.625$, $U_{TB} = 0.81$, $L_{TB} = 2.5 D_t$; (■) $U_{SL} = 0.714$, $U_{TB} = 0.90$, $L_{TB} = 2.7 D_t$; (△) $U_{SL} = 1.0$, $U_{TB} = 1.2$, $L_{TB} = 2.5 D_t$; (•) $U_{SL} = 1.25$, $U_{TB} = 1.44$, $L_{TB} = 2.6 D_t$; (—) $U_{SL} = 1.42$, $U_{TB} = 1.63$, $L_{TB} = 2.7 D_t$; x—axial distance from bubble nose; the frame of reference is as seen by a fixed observer.

bubble moving inside a 20 mm diameter tube. The frame of reference is as seen by a fixed observer and not moving with the bubble. The character of the wall shear stress distribution is similar for all cases. The wall shear stress sign changes twice in a slug unit. The first change takes place near the nose of the Taylor bubble and the second near the top of the liquid plug. The negative shear stress, indicating upflow, exists over the liquid plug ahead of the bubble and persists beyond the nose of the Taylor bubble, before becoming positive as the downflow is established in the liquid film around the bubble.

As the liquid flow increases, the portion of downward flow becomes shorter and the sign does not change if the bubble is not long enough ($U_{TB} = 1.63$). This is expected as the velocity of the Taylor bubble increases with increasing liquid velocity, and to accelerate the falling liquid film up to the velocity of the bubble (which corresponds to a zero wall shear stress in the bubble region) it is necessary that the bubble length to be long enough. Near the bubble tail fluctuations of the wall shear stress can be seen corresponding to the stirring nature of the wake trailing the bubble. This mixing zone caused by the annular film impinging the liquid plug behind the bubble plays a pivotal role in mass and heat transfer augmentation. The length of the mixing zone can be determined from the wall shear stress profile and found to be approximately $2D_t$ confirming the experimental findings of other researchers (Nakoryakov et al., 1989; Mao and Duckler, 1989).

3.3. Effect of angle of inclination

Although upward vertical two-phase slug flow has received considerably more attention in the open literature than downward and inclined flows for the obvious reason that the symmetry with respect to the tube axis is lost once the tube is tilted away from the vertical. The difficulty in handling the 3D nature of the flow limits the existence of experimental data. When the tube is titled away from the vertical, the axisymmetry of slug flow is breached. The degree of this eccentricity increases when the inclination increases from the vertical to the horizontal. Fig. 13 shows the shape and the velocity field around a Taylor bubble rising through motionless water in a 20 mm diameter tube when the tube is tilted 20° away from the vertical. This feasibility study of inclined slug flow shows that the VOF method adopted in this work proved to be powerful in tackling 3D slug flows, in general, and should meet the challenges in downward and inclined slug flow to provide a comprehensive picture of such complex flows.

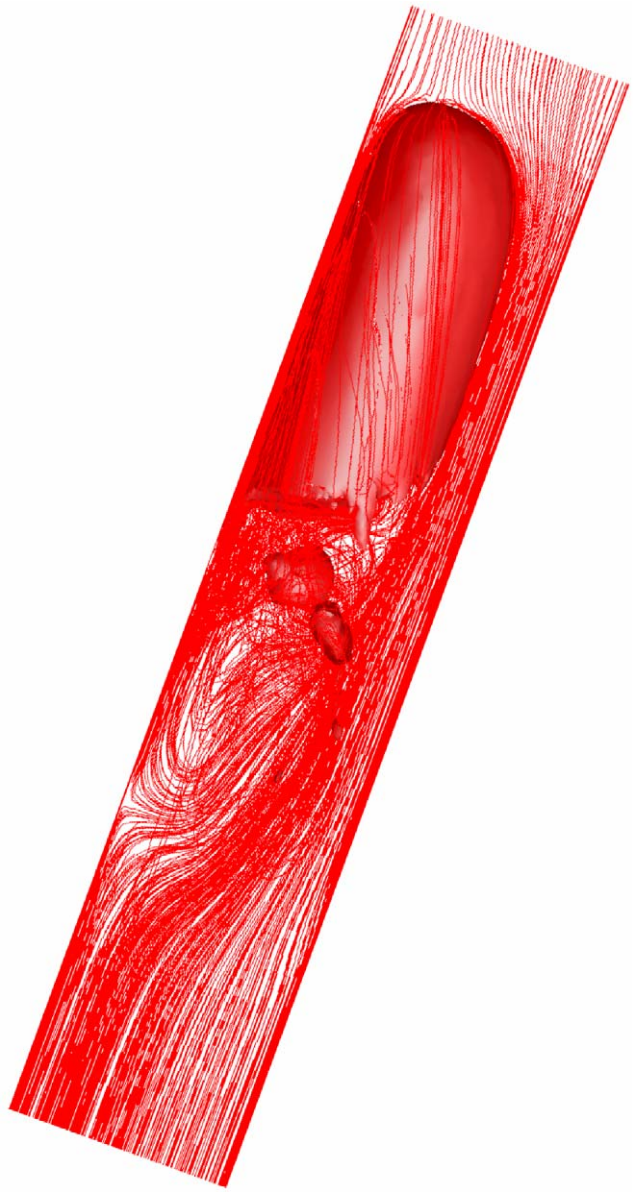

Fig. 13. Numerical simulation of a Taylor bubble rising through water inside a 20 mm diameter tube titled 20° away from the vertical.

4. Conclusions

In this paper we presented a numerical study to investigate the motion of single Taylor bubbles in vertical tubes. A complete description of the bubble propagation in both stagnant and flowing liquids was obtained. The bubble was found to have a cylindrical body with a spherical nose and a fluctuating tail. Sometimes, small bubbles were seen to be sheered off the tail due to the liquid jet coming down from the annular region that separates the bubble from the tube walls. As the bubble moves up, the liquid ahead of it is picked up, and at a certain distance from the bubble nose, it starts to accelerate downwards in the annular region. This distance becomes longer for faster bubbles. Under the condition of a long enough bubble, the liquid film accelerates until it eventually reaches its terminal velocity. At the rear of the bubble, the liquid film impinges the liquid plug behind the bubble as a circular wall jet and produces a highly agitated mixing zone in the bubble wake. Depending upon the inverse viscosity dimensionless number, N_f, the wake takes on different patterns.

When $N_f < 500$, the wake was found to be composed of two closed toroidal vortices which are mirror image of each other. The wake is enveloped into the oblate bubble tail. At $500 < N_f < 1500$, the bubble tail is nearly flat and the wake, still closed, tends to lose symmetry around the tube axis and to show periodic undulation, the frequency of which increases with increasing N_f. At $N_f > 1500$, the bubble wake opens and turbulent eddies are shed from the main bubble wake. For the low and moderate range of N_f, the length of the bubble wake was found to be linearly dependent on N_f.

The bubble shape was found to be dependent upon liquid viscosity and surface tension but not on the bubble length. The degree of prolateness of the nose and oblateness of the tail increase with surface tension. A wavelet was seen at the bubble tail when viscosity is high. The film thickness around the bubble decreases as surface tension increases. The bluntness of the bubble nose increases with decreasing viscosity, which results in an increment of the liquid thickness. The bubble velocity was calculated over a wide range of tube diameter and liquid properties and the values obtained compared favourably with experimental results reported in literature.

Notation

Ar	Archimedes number, dimensionless
C_1	dimensionless coefficient, dimensionless
C_f	dimensionless coefficient, dimensionless
Ca	capillary number, dimensionless
D_t	diameter of the tube, m
Eo	Eötvös number, dimensionless
f_w	friction factor, dimensionless
F_f	liquid holdup in the liquid film, dimensionless
Fr	Froude number, dimensionless
g	acceleration due to gravity, m/s^2
h	liquid film thickness, m
L_{LP}	length of liquid plug, m
L_{TB}	length of Taylor bubble, m
m	dimensionless coefficient, dimensionless
M	Morton number, dimensionless
N_f	inverse viscosity dimensionless number, dimensionless
R	bubble radius, m
U_0	Taylor bubble drift velocity, m/s
U_f	liquid film velocity, m/s
U_{inlet}	inlet velocity, m/s
U_m	mixture velocity, m/s
U_{SG}	superficial gas velocity, m/s
U_{SL}	superficial liquid velocity, m/s
U_{TB}	Taylor bubble velocity, m/s
U_{wall}	wall velocity, m/s
x	axial coordinate, m

Greek letters

α_G	volume fraction of the gas phase in the computational cell, dimensionless
μ_G	gas molecular viscosity, kg/m s
μ_L	liquid molecular viscosity, kg/m s
v	kinematic viscosity, m^2/s
ρ_G	gas density, kg/m^3
ρ_L	liquid density, kg/m^3
σ	surface tension, N/m

Acknowledgements

T. Taha is grateful to the Karim Rida Said Foundation for financial support and to Dr. David Kenning for helpful suggestions. This work is partially sponsored by EPSRC (GR/66438).

References

Ahmad, W., DeJesus, J.M., Kawaji, M., 1998. Falling film hydrodynamics in slug flow. Chemical Engineering Science 53, 123–130.

Barnea, D., 1987. A unified model for predicting flow pattern transition in the whole range of pipe inclination. International Journal of Multiphase Flow 13, 1–12.

Bendiksen, K.H., 1984. An experimental investigation of the motion of the long bubble in inclined tubes. International Journal of Multiphase Flow 10, 467–483.

Bendiksen, K.H., 1985. On the motion of long bubbles in vertical tubes. International Journal of Multiphase Flow 11, 797–812.

Brackbill, J.U., Kothe, D.B., Zemach, C., 1992. A continuum method for modeling surface tension. Journal of Computational Physics 100, 335–354.

Bretherton, F.P., 1961. The motion of long bubbles in tubes. Journal of Fluid Mechanics 10, 166–188.

Campos, J.B.L.M., Guedes de Carvalho, J.R.F., 1988. An experimental study of the wake of gas slugs rising in liquids. Journal of Fluid Mechanics 196, 27–37.

Clarke, A., Issa, R., 1997. A numerical model of slug flow in vertical tubes. Computers and Fluids 26, 395–415.

Collins, R., De Moraes, F.F., Davidson, J.F., Harrison, D., 1978. The motion of a large gas bubble rising through liquid flowing in a tube. Journal of Fluid Mechanics 89, 497–514.

Davies, R.M., Taylor, G., 1950. The mechanics of large bubble rising through extended liquids and through liquids in tubes. Proceedings of the Royal Society of London, Series A 200, 375–390.

DeJesus, J.D., Ahmed, W., Kawaji, M., 1995. Experimental study of flow structure in vertical slug flow. Proceedings of the Second International Conference Multiphase Flow, Kyoto, vol. 4. pp. 51–559.

Duckler, A.E., Hubbard, M.G., 1975. A model for gas liquid slug flow in horizontal and near horizontal tubes. Industrial and Engineering Chemistry Fundamentals 14, 337–347.

Duckler, A.E., Maron, D.M., Brauner, N., 1985. A physical model for predicting the minimum stable slug length. Chemical Engineering Science 40, 1379–1386.

Dumitrescu, D.T., 1943. strömung an einer Luftblase im senkrechten Rohr. Zeitschrift fuer Angewandte Mathematik und Mechanik 23, 139–149.

Fabre, J., Line, A., 1992. Modelling of two-phase slug flow. Annual Review of Fluid Mechanics 24, 21–46.

Gibson, A.H., 1913. On the motion of long air-bubbles in a vertical tube. Philosophical Magazine 26, 952.

Goldsmith, H.L., Mason, S.G., 1962. The movement of single large bubbles in closed vertical tubes. Journal of Fluid Mechanics 14, 42–58.

Grace, J.R., Clift, R., 1979. Dependence of slug rise velocity on tube Reynolds number in vertical gas–liquid flow. Chemical Engineering Science 34, 1348–1350.

Griffith, P., Wallis, G.B., 1961. Two-phase slug flow. Journal of Heat Transfer 83, 307–320.

Harmathy, T.Z., 1960. Velocity of large drops and bubbles in media of infinite or restricted extent. A.I.Ch.E. Journal 6, 281–288.

Hattori, S., 1935. Report, Aeronautical Research Institute, Tokyo Imperial University, No. 115.

Hewitt, G.F., Hall-Taylor, N.S., 1970. Annular Two-phase Flow. Pergamon Press, London.

Hirt, C.W., Nichols, B.D., 1981. Volume of fluid (VOF) method for the dynamics of free boundaries. Journal of Computational Physics 39, 201–225.

Kawaji, M., DeJesus, J.M., Tudsoe, G., 1997. Investigation of flow structures in vertical slug flow. Nuclear Engineering and Design 175, 37–48.

Kvernvold, O., Vindoy, V., Sontvedt, T., Saasen, A., Selmen-Oslen, S., 1984. Velocity distribution in horizontal slug flow. International Journal of Multiphase Flow 10, 441–457.

Laird, A.D., Chisholm, D.A., 1956. Pressure and forces along cylindrical bubbles in vertical tube. Journal of Industrial and Engineering Chemistry 48, 1361.

Lighthill, M.J., 1968. Pressure-forcing of tightly pellets along fluid-filled elastic tubes. Journal of Fluid Mechanics 34, 251–272.

Mandhane, J.M., Gegory, G.A., Aziz, K., 1974. A flow pattern map for gas–liquid flow in horizontal pipes. International Journal of Multiphase Flow 1, 537–553.

Mao, Z.S., Duckler, A.E., 1989. An experimental study of gas–liquid slug flow. Experiments in Fluids 8, 169–182.

Mao, Z.S., Duckler, A.E., 1990. The motion of Taylor bubbles in vertical tubes—I. A numerical simulation for the shape and the rise velocity of Taylor bubbles in stagnant and flowing liquids. Journal of Computational Physics 91, 132–160.

Mao, Z.S., Duckler, A.E., 1991. The motion of Taylor bubbles in vertical tubes: II. Experimental data and simulations for laminar and turbulent flow. Chemical Engineering Science 46, 2055–2064.

Martin, C.S., 1976. Vertically downward two-phase slug flow. Journal of Fluids Engineering 98, 715–722.

Maxworthy, T., 1967. A note on the existence of wakes behind large rising bubbles. Journal of Fluid Mechanics 27, 367–368.

Moissis, R., Griffith, P., 1962. Entrance effect in a two-phase slug flow. Journal of Heat Transfer 84, 29–39.

Nakoryakov, V.E., Kashinsky, O.N., Petukhov, A.V., Gorelik, R.S., 1989. Study of local hydrodynamic characteristics of upward slug flow. Experiments in Fluids 7, 560–566.

Nicklin, D.J., Wilkes, J.O., Davidson, J.F., 1962. Two-phase flow in vertical tubes. Transactions of the Institution of Chemical Engineers 40, 61–68.

Nogueria, S., Dias, I., Pinto, A.M.F.R., Riethmuller, M.L., 2000. Liquid PIV measurements around a single gas slug rising through stagnant liquid in vertical pipes. Tenth Symposium on Laser Techniques Applied to Fluid Mechanics, Lisbon.

Pinto, A.M.F.R., Campos, J.B.L.M., 1996. Coalescence of two gas slugs in rising in a vertical column of liquid. Chemical Engineering Science 51, 45–54.

Polonsky, S., Shemer, L., Barnea, D., 1999. The relation between the Taylor bubble motion and the velocity field ahead of it. International Journal of Multiphase Flow 25, 957–975.

Shemer, L., Barnea, D., 1987. Visualization of the instantaneous velocity profiles in gas-liquid slug flow. PhysicoChemical Hydrodynamics 8, 243–253.

Taitel, Y., 1986. Stability of severe slugging. International Journal of Multiphase Flow 12, 203–217.

Taitel, Y., Barnea, D., 1990. Two-phase slug flow. Advances in Heat Transfer 20, 83–132.

Taitel, Y., Duckler, A.E., 1976. A model for predicting flow regime transitions in horizontal and near horizontal gas–liquid flow. A.I.Ch.E. Journal 22, 47–55.

Talvy, C.A., Shemer, L., Barnea, D., 2000. On interaction between leading and trailing elongated bubbles in a vertical pipe flow. International Journal of Multiphase Flow 26, 1905–1923.

van Hout, R., Gulitski, A., Barnea, D., Shemer, L., 2002. Experimental investigation of the velocity field induced by a Taylor bubble rising in stagnant water. International Journal of Multiphase Flow 28, 579.

Wallis, G.B., 1969. One-dimensional Two-phase Flow. McGraw Hill, New York.

Weber, M.E., Alarie, A., Ryan, M.E., 1986. Velocities of extended bubbles in inclined tubes. Chemical Engineering Science 41, 2235–2240.

White, E.T., Beardmore, R.H., 1962. The velocity of rise of single cylindrical air bubbles through liquids contained in vertical tubes. Chemical Engineering Science 17, 351–361.

Youngs, D.L., 1982. Time-dependent multi-material flow with large fluid distortion. In: Morton, K.W., Baibnes, M.J. (Eds.), Numerical Methods for Fluid Dynamics. Academic Press, New York, p. 273.

Zukoski, E.E., 1966. Influence of viscosity, surface tension, and inclination angle on motion on long bubbles in closed tubes. Journal of Fluid Mechanics 25, 821–837.